Physics of Fluids

Bathymetry and friction estimation from transient velocity data for one-dimensional shallow water flows in open channels with varying width

Cite as: Phys. Fluids **35**, 027109 (2023); https://doi.org/10.1063/5.0136017
Submitted: 23 November 2022 • Accepted: 16 January 2023 • Accepted Manuscript Online: 18 January 2023 • Published Online: 07 February 2023

Gerardo Hernández-Dueñas, Miguel Angel Moreles and Pedro González-Casanova

Physics of Fluids ARTICLE scitation.org/journal/phf

Bathymetry and friction estimation from transient velocity data for one-dimensional shallow water flows in open channels with varying width

Cite as: Phys. Fluids **35**, 027109 (2023); doi: 10.1063/5.0136017
Submitted: 23 November 2022 · Accepted: 16 January 2023 ·
Published Online: 7 February 2023

View Online Export Citation CrossMark

Gerardo Hernández-Dueñas,[1] Miguel Angel Moreles,[2,a)] and Pedro González-Casanova[3]

AFFILIATIONS

[1]Instituto de Matemáticas - Juriquilla, Universidad Nacional Autónoma de México, Blvd. Juriquilla 3001, Querétaro 76230, Mexico
[2]Centro de Investigación en Matemáticas, Jalisco s/n, Valenciana, Guanajuato, Gto 36240, Mexico
[3]Instituto de Matemáticas - CdMx, Universidad Nacional Autónoma de México, Área de la Investigación Científica, Circuito exterior, Ciudad Universitaria, 04510 Coyoacan, CDMX, Mexico

[a)]Author to whom correspondence should be addressed: moreles@cimat.mx

ABSTRACT

The shallow water equations (SWE) model a variety of geophysical flows. Flows in channels with rectangular cross sections may be modeled with a simplified one-dimensional SWE with varying width. Among other model parameters, information about the bathymetry and friction coefficient is needed for the correct and precise prediction of the flow. Although synthetic values of the model parameters may suffice for testing numerical schemes, approximations of the bathymetry and other parameters may be required for specific applications. Estimations may be obtained by experimental methods, but some of those techniques may be expensive, time consuming, and not always available. In this work, we propose to solve the inverse problem to estimate the bathymetry and the Manning's friction coefficient from transient velocity data. This is done with the aid of a cost functional, which includes the SWE through Lagrange multipliers. We prove that the velocity data determine uniquely the derivative of the bathymetry in a linearized shallow water system. That is, the inverse problem is identifiable. The solution is obtained by solving the constrained optimization problem by a continuous descent method. The direct and the adjoint problems are both solved numerically using a second-order accurate Roe-type upwind scheme. Numerical tests are included to show the merits of the algorithm.

I. INTRODUCTION

The shallow water equations (SWE) model a variety of geophysical flows, and a vast amount of applications exist in the literature. They can be derived from depth-integrating the Navier–Stokes equations in the case where the horizontal length scale is much greater than the vertical length scale. Our interest is in the one-dimensional shallow water approximation, also known as the St-Venant equations. We refer the reader to Refs. 1 and 2 and references therein for more details on shallow water theory and the inverse problem to be addressed here.

Direct problems for the shallow water systems, such as modeling inundation of small-scale coastal regions[3] or hydrodynamic modeling of open-channel flows, involve the solution of 1D shallow water systems.[4] Such a system has been intensively studied during the last decades. Computing the corresponding solutions requires the knowledge of the bed bathymetry, appropriate initial and boundary conditions, and possibly specific model parameters such as friction coefficients. The inverse problems of computing the bed bathymetry and/or the friction's coefficients from available data are currently an intensive research area where several works have been formulated to solve these problems under different situations. See, for example, Refs. 5–10 and references therein. We particularly mention the recent work[11] where the reconstruction of ocean bathymetry from the free surface velocity and elevation is proposed. Such approach is applied to real data.

In this work, we focus on the signature that the bathymetry leaves on the perturbations in transient flows given by the shallow water equations in open channels with vertical walls and varying width. This leads to the solution of an inverse problem to estimate the channel's bathymetry and Manning's friction coefficient from prescribed transient velocity data. To the best of our knowledge, this problem has not been addressed in the literature.

Estimating the bathymetry and Manning's friction coefficient from transient velocity measurements is considerably more challenging

compared to a situation where the flow corresponds to a steady state. In this work, using a cost functional constrained to the shallow water equations, we formulate an algorithm capable of recovering the bathymetry from a set of point values of the fluid's velocity in the channel. Specifically, we formulate a cost functional that includes the SWE through Lagrange multipliers. Boundary and initial conditions are included. The constrained optimization problem is solved by a continuous descent method. Namely, the gradient is computed analytically by the adjoint state method, then discretized. Several benchmark problems are presented in order to verify the numerical performance of the proposed method.

The paper is organized as follows. In Sec. II, the bathymetry model and the friction estimation problem are studied. We prove that the velocity data determine uniquely the derivative of the bathymetry in a linearized shallow water system. That is, the inverse problem is identifiable. Due to the hyperbolic character of the system, the speed of propagation of the data is finite. Thus, we obtain here an estimate for the time at which we need to observe the data. This time is used successfully in the nonlinear case, except in those cases where both the bathymetry and the Manning's friction coefficients are estimated simultaneously. In Sec. III, the constrained optimization problem is solved by a continuous descent method. Namely, the gradient is computed analytically, then discretized. In Sec. IV, we develop well-balanced Roe-type upwind schemes for the direct and adjoint problems in the adjoint state method. The schemes follow closely the one introduced in Ref. 12 to solve the direct problem for the transient shallow water system in the case of channels with varying width. In Sec. V, the performance of the techniques presented in this paper is numerically verified for different problems. Specifically, we consider different situations to argue on the merits and robustness of the algorithm.

II. THE BATHYMETRY AND FRICTION ESTIMATION PROBLEM

A. The inverse problem

The underlying physical problem deals with water flows in rectangular channels with irregular bathymetry, varying width, and friction. The model is the 1D SWE,[13] which is written as a hyperbolic balance law as

$$\begin{pmatrix} \sigma h \\ \sigma hu \end{pmatrix}_t + \begin{pmatrix} \sigma hu \\ \sigma hu^2 + \frac{g}{2}\sigma h^2 \end{pmatrix}_x = \begin{pmatrix} 0 \\ \frac{1}{2}gh^2\sigma_x - g\sigma hB_x - gn^2\frac{\sigma h}{R^{4/3}}u|u| \end{pmatrix}, \quad a < x < b, \ t > 0. \tag{1}$$

Here, h is the depth of the layer, u is the velocity, $B(x)$ is the bathymetry, $\sigma(x)$ is the channel's width at position x, $g = 9.81\,\mathrm{m\,s^{-2}}$ is the acceleration of gravity, n is the Manning's friction coefficient, and $R = \frac{\sigma h}{\sigma + 2h}$ is the hydraulic radius. The hydraulic radius is the ratio of the wet area and the wetted perimeter. See Ref. 14 for more details on the friction term. Figure 1 shows the schematic of the model. The velocity is in units of meters per second, while x, h, σ are in units of meters and time in seconds. The friction coefficient is in units of $\mathrm{s\,m^{-1/3}}$.

There exists a variety of techniques to measure the velocity in open channels. See, for instance, Ref. 15, where river discharge estimations and measurements of velocity using an aircraft system are analyzed. The inverse problem to solve is stated as follows:

Assume that the cross-sectional velocity u is measured at the points $(x_j, t_k), j = 1, 2, \ldots, N, k = 1, 2, \ldots, K$. Namely, $u(x_j, t_k) \approx \hat{u}_{j,k}$. With these velocity data, it is possible find an estimation of the bathymetry $B \equiv B(x)$ and Manning's friction coefficient n, in the 1D SWE.

B. The observation time for a linearized SWE—A theoretical result

The interest here is to prove that the velocity data determine uniquely the bathymetry and the Manning coefficient. That is, the inverse problem is identifiable. Let us consider a channel with constant width and no friction, then an identifiability result is valid for a linearized SWE. In this case, we obtain an estimate for the time at which we need to observe the data. Specifically, for a flat bathymetry at depth H and domain size L, the time required for the observed data is determined by the speed of propagation, consequently given by $T = \frac{L}{\sqrt{gH}}$. As we will see below, this same time has shown to be a good estimate for the nonlinear cases, except for the numerical tests where we are also estimating the Manning's friction coefficient.

Let us derive the observation time in the linear case. The simplified equation, constant width, and no friction, reads

$$\begin{pmatrix} h \\ hu \end{pmatrix}_t + \begin{pmatrix} hu \\ hu^2 + \frac{g}{2}h^2 \end{pmatrix}_x = \begin{pmatrix} 0 \\ -ghB_x \end{pmatrix}. \tag{2}$$

Let h be a perturbation of H, namely,

$$h = \eta + H, \quad |\eta| \ll H.$$

Substituting η_t from the first equation on the second, and disregarding second-order terms, we obtain

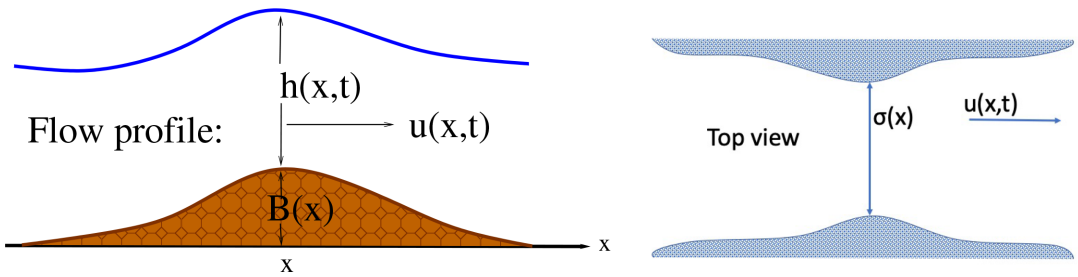

FIG. 1. Schematic of the shallow water model. The left panel shows the flow profile along the channel. The right panel shows the top view.

$$\begin{pmatrix}\eta\\ u\end{pmatrix}_t+\begin{pmatrix}Hu\\ g\eta\end{pmatrix}_x=\begin{pmatrix}0\\ -\frac{g}{H}(\eta+H)B_x\end{pmatrix}. \tag{3}$$

The flux and its derivative are

$$F_L(\eta,u)=\begin{pmatrix}Hu\\ g\eta\end{pmatrix},\quad DF_L(\eta,u)=\begin{pmatrix}0 & H\\ g & 0\end{pmatrix}.$$

The eigenvalues of the latter are $\pm\sqrt{gH}$, hence, the speed of propagation $\sqrt{gH}$.

For identifiability, set $C=B_x$. Assume that given C_1 and C_2 there is a common solution (η,u). Then, in the second equation of (3), we have

$$(\eta(x,t)+H)(C_1(x)-C_2(x))=0.$$

Assume there is an interval $(a,\ b)$ such that $C_1(x)\neq C_2(x)$, $a<x<b$, then on that interval, $\eta(x,t)=-H$, which is an impossibility.

The slope of the characteristics are $\pm1/\sqrt{gH}$. Hence, for a domain of length L, the solution will contain all information at $(x,\ t)$ for $t\geq T=\frac{L}{\sqrt{gH}}$.

Let us recall a general uniqueness result for first-order hyperbolic systems in the form

$$\mathbf{u}_t+\mathbf{A}(\mathbf{u})\mathbf{u}_x=0. \tag{4}$$

Assume that in a neighborhood of $\mathbf{0}$, the matrix $\mathbf{A}(\mathbf{u})$ has real eigenvalues

$$\lambda_1(\mathbf{u})<\lambda_2(\mathbf{u})<\ldots<\lambda_N(\mathbf{u}).$$

Theorem 1. *If $\mathbf{u}\in C^2$ satisfies (4) for $0\leq t\leq T$ and $\mathbf{u}(x,0)=\mathbf{0}$ for $\alpha\leq x\leq\beta$, then $\mathbf{u}(x,t)=\mathbf{0}$, where $0\leq t<T$ and $\alpha+\lambda_N(\mathbf{0})t\leq x\leq\beta+\lambda_1(\mathbf{0})t$.*

Proof. Theorem 4.2.2 Hörmander in Ref. 16. □

In our case, we start by writing Eq. (2) in the form

$$\begin{pmatrix}h\\ u\end{pmatrix}_t+\begin{pmatrix}hu\\ \frac{1}{2}u^2+gh\end{pmatrix}_x=\begin{pmatrix}0\\ -gB_x\end{pmatrix}, \tag{5}$$

and in terms of η, we get

$$\begin{pmatrix}\eta\\ u\end{pmatrix}_t+\begin{pmatrix}(\eta+H)u\\ \frac{1}{2}u^2+g(\eta+H)\end{pmatrix}_x=\begin{pmatrix}0\\ -gB_x\end{pmatrix}. \tag{6}$$

Differentiating with respect to x, we have

$$\begin{pmatrix}\eta\\ u\end{pmatrix}_t+\begin{pmatrix}u & \eta+H\\ g & u\end{pmatrix}\begin{pmatrix}\eta\\ u\end{pmatrix}_x=\begin{pmatrix}0\\ -gB_x\end{pmatrix}. \tag{7}$$

The corresponding matrix is

$$A(\eta,u)=\begin{pmatrix}u & \eta+H\\ g & u\end{pmatrix}$$

and

$$\mathbf{A}(0,0)=\begin{pmatrix}0 & H\\ g & 0\end{pmatrix}.$$

Consequently, $\lambda_1(\mathbf{0})=-\sqrt{gH}$, $\lambda_N(\mathbf{0})\equiv\lambda_2(\mathbf{0})=\sqrt{gH}$, and the speed of propagation coincides with the linear equation for smooth solutions.

We summarize the results as follows:

Theorem 2. *If $\mathbf{u}\in C^2$ satisfies (7) for $0\leq t\leq T$ and $\mathbf{u}(x,0)=\mathbf{0}$ for $\alpha\leq x\leq\beta$, then $\mathbf{u}(x,t)=\mathbf{0}$, where $0\leq t<T$ and $\alpha+\sqrt{gH}\,t\leq x\leq\beta-\sqrt{gH}\,t$.*

Notice that in the linear case in this Theorem 2, we are using implicitly the existence of a global solution, locally smooth, with discontinuities propagating along the characteristics. In the nonlinear case, a global solution only exits weakly. See, for instance, Liu and Yang.[17]

III. SOLUTION BY A CONTINUOUS DESCENT METHOD

In this section, we formulate the inverse problem as a minimization problem, and we develop the continuous descent method for its solution. We follow a functional approach, that is, we optimize on Hilbert spaces of functions using Fréchet differentiation. We refer to Ref. 18 for this and other methods of applied analysis to be used in the sequel.

Let the bathymetry B, and Manning's coefficient n, be given. The corresponding solution u of the St.-Venant equations is written as $u(x,t;B,n)$.

Consider the bathymetry B as a function defined on an interval $(a,\ b)$ belonging to the Hilbert space of square integrable functions $L^2(a,b)$. Since Manning's coefficient is a real number, it is natural to introduce the least squares functional,

$$\begin{aligned}J:L^2(a,b)\times\mathbb{R}&\to\mathbb{R},\\ (B,n)&\mapsto J(B,n),\end{aligned} \tag{8}$$

given by

$$J(B,n)=\frac{1}{2}\sum_{j,k}\left(u(x_j,t_k;B,n)-\hat{u}_{j,k}\right)^2. \tag{9}$$

Our goal is to minimize J constrained to h, u solving the shallow water system (1).

The constrained optimization problem is solved by a continuous descent method. Namely, the gradient is computed analytically, then discretized.

A. The analytic gradient

Using the adjoint state method, let us construct an expression of the gradient of J.

Let $\langle\cdot,\cdot\rangle_{L^2(\Omega\times(0,T))}$ be the normalized inner product in $L^2(\Omega\times(0,T))$, given by

$$\langle f,g\rangle_{L^2(\Omega\times(0,T))}=\frac{1}{(b-a)T}\int_0^T\int_a^b f(x,t)\overline{g(x,t)}\,dxdt.$$

Here, $\Omega=(a,b)$.

Let u be a continuous function defined on $\Omega\times(0,T)$, $[u\in C(\Omega\times(0,T))]$. Consider the (linear) observation operator

$$\begin{aligned}\mathscr{M}:C(\Omega\times(0,T))\subset L^2(\Omega\times(0,T))&\to\mathbb{R}^{N\times K},\\ \mathscr{M}u&=\{u(x_j,t_k)\}.\end{aligned} \tag{10}$$

For later reference, let us recall the adjoint operator $\mathscr{M}^*$, which satisfies

$$\langle \mathscr{M} f, g\rangle_{\mathbb{R}^{N\times K}} = \langle f, \mathscr{M}^* g\rangle_{L^2(\Omega\times(0,T))}.$$

We have Cauchy data

$$u(x,0) = u_0(x), \quad h(x,0) = h_0(x), \quad a < x < b.$$

For definiteness, assume a left inflow boundary where discharge, $Q = hu$, and surface w are specified. Here, $h = w - B$.

In terms of the observation operator, the functional J becomes

$$J(B,n) = \frac{1}{2}||\mathscr{M}u(\cdot,\cdot;B,n) - \hat{u}||^2,$$

where $||\cdot||$ is the Euclidean norm on $\mathbb{R}^{N\times K}$.

Let us also consider the Lagrangian

$$\mathscr{L}(B,n,h,u;\lambda,\mu) = \frac{1}{2}||\mathscr{M}u - \hat{u}||^2 + \left\langle \begin{pmatrix}\lambda\\ \mu\end{pmatrix}, \begin{pmatrix} (\sigma h)_t + (\sigma h u)_x \\ (\sigma h u)_t + (\sigma h u^2 + \frac{g}{2}\sigma h^2)_x - \frac{g}{2}h^2\sigma_x + g\sigma h B_x + gn^2\frac{\sigma h}{R^{4/3}}u|u| \end{pmatrix} \right\rangle_{L^2(\Omega\times(0,T))}, \tag{11}$$

where λ and μ are Lagrange multipliers.

Consider h, u solutions of the St-Venant equations as functions of (B, n). Then, regardless of the Lagrange multipliers, J can be written as the composition

$$J(B,n) = \mathscr{L} \circ (h,u)(B,n).$$

Assuming Fréchet differentiability, by the chain rule, it follows that

$$DJ(B,n) = D\mathscr{L}(h,u)D(h,u)(B,n). \tag{12}$$

Consequently, in the adjoint state method, one chooses appropriate Lagrange multipliers to obtain an expression for the gradient of J. In this case, we have the following:

Theorem 3. *Let B and n be given, and let h, u solve the shallow water equations. Suppose that the velocity measurements are taken in space and time $(x,t) \in [a,b]\times[0,T]$ for $T > 0$. Furthermore, assume the Lagrange multipliers solve the adjoint equations*

$$\begin{aligned} &\sigma\lambda_t + \sigma u\lambda_x + \sigma u\mu_t + (\sigma u^2 + g\sigma h)\mu_x \\ &+ \left(gh\sigma_x - g\sigma B_x - gn^2\left(\frac{1}{h}+\frac{2}{\sigma}\right)^{1/3}\left(2 - \frac{1}{3}\frac{\sigma}{h}\right)u|u|\right)\mu = 0 \\ &\sigma h\mu_t + 2\sigma h u\mu_x + \sigma h\lambda_x - gn^2\frac{\sigma h}{R^{4/3}}2|u|\mu = \mathscr{M}^*(\mathscr{M}u - \hat{u}) \end{aligned} \tag{13}$$

with final and boundary conditions

$$\lambda(x,T) = 0, \quad \mu(x,T) = 0, \quad x \in (a,b) \tag{14}$$

and

$$\lambda(b,t) = 0, \quad \mu(b,t) = 0. \quad t \in (0,T). \tag{15}$$

Then the Fréchet derivative of the functional J is

$$DJ(B,n)(\xi_1,\xi_2) = \langle \xi_1, -\int_0^T (g\sigma h\mu)_x\, dt\rangle + \langle \mu, 2g\, n\frac{\sigma h}{R^{4/3}}u|u|\rangle\xi_2.$$

Consequently,

$$\nabla J(B,n) = \begin{pmatrix} -\overline{(g\sigma h\mu)}_x \\ \langle \mu, 2g\, n\frac{\sigma h}{R^{4/3}}u|u|\rangle \end{pmatrix}.$$

Here, $\overline{(\cdot)}$ denotes the time average

$$\bar{f}(x) = \frac{1}{T}\int_0^T f(x,t)dt.$$

The proof is classical and straightforward. The chain rule (12) is computed applying basic Fréchet differentiation rules, then integrating by parts to construct the adjoint system. See Ref. 2 and references therein.

We note that if the direct problem is solved for times $t \in [0,T]$ with initial conditions at $t = 0$ as specified in Sec. V, the adjoint problem has zero final conditions at time $t = T$, and the solution is computed backward in time from $t = T$ to $t = 0$.

B. A line search method

The bathymetry and Manning's friction coefficient are inferred iteratively. We start with an initial guess, which in principle must be not too far from the target. In each step, one computes the gradient and advances in the steepest search direction. The amplitude to advance in the steepest direction is initially obtained empirically. One then modulates it to minimize the error. We continue iteratively until an error threshold is achieved. The algorithm is summarized as follows.

Algorithm (Continuous descent). Given a starting point B_0 and n_o, a convergence tolerance ε, and $k \leftarrow 0$; while $||\nabla J(B_k, n_k)|| > \varepsilon$;

Compute the steepest search direction

$$p_k = (p_{1,k}, p_{2,k}) = -\nabla J(B_k, n_k). \tag{16}$$

Here, $p_{1,k}$ and $p_{2,k}$ are, respectively, the descent directions corresponding to the bathymetry and the Manning's coefficient, at iteration k. Set

$$B_{k+1} = B_k + \alpha_k p_{1,k}; \quad n_{k+1} = n_k + \alpha_k p_{2,k}; \tag{17}$$

$k \leftarrow k+1$; end (while)

Since

$$\nabla J(B,n) = \begin{pmatrix} -\overline{(g\sigma h\mu)}_x \\ \langle \mu, 2g\frac{\sigma h}{R^{4/3}}u|u|\rangle \end{pmatrix},$$

we have

$$p_k = \begin{pmatrix} \overline{(g\sigma h\mu)}_x \\ -\langle \mu, 2g\dfrac{\sigma h}{R^{4/3}}u|u|\rangle \end{pmatrix}.$$

We recall that the overline denotes the time average. The steepest search direction for the bathymetry is a function of x only, and a constant for Manning's friction coefficient. At each iteration step where p_k from Eq. (16) is already computed, we choose the coefficient α_k in Eq. (17) as follows. One starts with an initial value ($\alpha_k = 0.5$ unless otherwise noted) and computes (B_{k+1}, n_{k+1}) according to Eq. (17). One then calculates the error in the velocity with that estimated bathymetry. If the error decreases when α_k is reduced by a certain factor (0.8 here), we keep reducing it until the error does not decrease any more.

Also note that when either the Manning's friction coefficient or the bathymetry is known, we can estimate the other parameter by considering only one of the entries in p_k.

IV. NUMERICAL METHODS

A. A Roe-type scheme for the hyperbolic systems (1) and (13)

A wide variety of numerical schemes have been proposed to solve the shallow water equations. Such schemes use different approaches and satisfy desirable properties for different goals. In Ref. 12, a Roe-type well-balanced numerical scheme is proposed. That is, it exactly preserves steady sates at rest, adding accuracy when computing near steady-state flows. Imposing appropriate boundary conditions could lead to a convergence to transcritical discontinuous steady states where the discharge is constant but the energy is piece-wise constant. Roe-type well-balanced upwind schemes are known to be very precise near those flows even in the presence of shockwaves. See, for instance, Fig. 6 in Ref. 19, where the numerical approximations for both the discharge and energy are plotted. The central-upwind scheme presented in Ref. 20 satisfies both the well-balanced and the positivity-preserving properties. That is, it recognizes steady states at rest, and it maintains the positivity of layer's depth over time. Many other approaches have also been studied. We refer the interested reader to the above works and references therein for more information.

1. The direct problem

In quasilinear form, it is well known (see, e.g., Ref. 21) that system (1) can be written as

$$\mathbf{W}_t + A\mathbf{W}_x = \mathbf{S}, \tag{18}$$

where

$$\mathbf{W} = \begin{pmatrix} \sigma h \\ \sigma hu \end{pmatrix}, \quad A = \begin{pmatrix} 0 & 1 \\ c^2 - u^2 & 2u \end{pmatrix}, \quad \text{and} \quad \mathbf{S} = \begin{pmatrix} 0 \\ -g\sigma hB_x + gh^2\sigma_x - \dfrac{gn^2A}{R^{4/3}}|u|u \end{pmatrix} \tag{19}$$

are the vector of conserved variables, the coefficient matrix, and the vector of source terms, respectively. The coefficient matrix has eigenvalues $\lambda_1 = u - c, \lambda_2 = u + c$, and corresponding eigenvectors $r_1 = (1, u - c)^T$ and $r_2 = (1, u + c)^T$, where $c = \sqrt{gh}$. As a result, system (1) is conditionally hyperbolic provided $h > 0$. Hyperbolicity is lost when $h = 0$ in a dry state.

Roe-type upwind schemes were first introduced in Ref. 22. The numerical scheme requires the computation of a Roe matrix $\bar{A}(\mathbf{W}_\ell, \mathbf{W}_r)$ for any left and right states $\mathbf{W}_\ell$ and $\mathbf{W}_r$. The flux $\mathbf{F} = \mathbf{F}(W, \sigma) = \left(\sigma hu, \sigma hu^2 + \frac{g}{2}\sigma h^2\right)^T$ of the model in conservation form (1) depends explicitly not only on the solution variables but also on the model parameter σ. For such flux, the Roe matrix $\bar{A}(\mathbf{W}_\ell, \mathbf{W}_r)$ must satisfy $\bar{A}(\mathbf{W}_\ell, \mathbf{W}_r) \to A(\mathbf{W})$ as $\mathbf{W}_\ell, \mathbf{W}_r \to \mathbf{W}$, it must have real eigenvalues with a complete set of eigenvectors, and

$$\Delta\mathbf{F} = \bar{A}(\mathbf{W}_\ell, \mathbf{W}_r)\Delta\mathbf{W} + \left(0, -g\bar{h}^2\Delta\sigma/2\right)^T, \tag{20}$$

where $\Delta\mathbf{F} = \mathbf{F}(\mathbf{W}_r) - \mathbf{F}(\mathbf{W}_\ell)$, $\Delta\mathbf{W} = \mathbf{W}_r - \mathbf{W}_\ell$, $\Delta\sigma = \sigma_r - \sigma_\ell$, and $\bar{h}$ is an approximation of h between the left and right states. One such matrix is given by the following Roe linearizations:

$$\bar{u} = \frac{\sqrt{\sigma_\ell h_\ell}\,u_\ell + \sqrt{\sigma_r h_r}\,u_r}{\sqrt{\sigma_\ell h_\ell} + \sqrt{\sigma_r h_r}}, \quad \bar{h} = \frac{\sqrt{\sigma_\ell}\,h_\ell + \sqrt{\sigma_r}\,h_r}{\sqrt{\sigma_\ell} + \sqrt{\sigma_r}}, \quad \text{and} \quad \bar{c} = \sqrt{g\bar{h}}.$$

In Ref. 12, a Roe-type upwind scheme is derived with the aid of a convenient discretization of the source terms that balance the flux gradients for steady states at rest. That is, the numerical scheme is well balanced. See Ref. 23 for more details. In order to extend it here for the case of channels with varying width, one possible discretization of the source terms is given by

$$\Delta x\,\bar{\mathbf{S}} = \begin{pmatrix} 0 \\ -g\bar{\sigma}\bar{h}\Delta B + g\bar{h}^2\Delta\sigma - \dfrac{gn^2\bar{\sigma}\bar{h}}{\bar{R}^{4/3}}|\bar{u}|\bar{u}, \end{pmatrix},$$

where

$$\bar{\sigma} = \sqrt{\sigma_\ell\sigma_r}, \quad \bar{R} = \frac{\bar{\sigma}\bar{h}}{\bar{\sigma} + 2\bar{h}}, \quad \Delta B = B_r - B_\ell, \quad \text{and} \quad \Delta\sigma = \sigma_r - \sigma_\ell.$$

Finite differences of the conserved variables and the linearized source terms are decomposed in terms of the eigenvectors $\bar{\mathbf{r}}_1 = (1, \bar{u} - \bar{c})^T$, $\bar{\mathbf{r}}_2 = (1, \bar{u} + \bar{c})^T$ as

$$\Delta\mathbf{W} = \alpha_1\bar{\mathbf{r}}_1 + \alpha_2\bar{\mathbf{r}}_2, \quad \Delta x\hat{\mathbf{S}} = \beta_1\bar{\mathbf{r}}_2 + \beta_1\bar{\mathbf{r}}_2,$$

where

$$\alpha_1 = \frac{-\Delta(\sigma hu) + (\bar{u} + \bar{c})\Delta(\sigma h)}{2\bar{c}},$$
$$\beta_1 = \frac{\bar{c}\bar{\sigma}}{2}\Delta B - \frac{\bar{c}\bar{h}}{2}\Delta\sigma + \frac{n^2\bar{c}\bar{\sigma}}{2\bar{R}^{4/3}}\Delta x\,|\bar{u}|\bar{u},$$
$$\alpha_2 = \frac{\Delta(\sigma hu) - (\bar{u} - \bar{c})\Delta(\sigma h)}{2\bar{c}},$$
$$\beta_2 = -\frac{\bar{c}\bar{\sigma}}{2}\Delta B + \frac{\bar{c}\bar{h}}{2}\Delta\sigma - \frac{n^2\bar{c}\bar{\sigma}}{2\bar{R}^{4/3}}\Delta x\,|\bar{u}|\bar{u}.$$

More details on the implementation of the numerical scheme can be found in Ref. 24. For the sake of completeness, we include some

details here. We denote by $\mathbf{W}_{j+\frac{1}{2}}$ the Roe averages between the states $\mathbf{W}_j$ and $\mathbf{W}_{j+1}$ in the domain with cells $I_j = [x_{j-\frac{1}{2}}, x_{j+\frac{1}{2}}]$, $x_{j\pm\frac{1}{2}} = x_j \pm \Delta x/2$. The second-order numerical scheme is given by

$$\begin{aligned}\mathbf{W}_j^{k+1} = \mathbf{W}_j^k &- \frac{\Delta t}{\Delta x}\sum_{\lambda^k_{j-1/2,p}>0}(\alpha^k_{j-1/2,p}\lambda^k_{j-1/2,p} - \beta^k_{j-1/2,p})\,\bar{\mathbf{r}}^k_{j-1/2,p} - \frac{\Delta t}{\Delta x}\sum_{\lambda^k_{j+1/2,p}<0}(\alpha^k_{j+1/2,p}\lambda^k_{j+1/2,p} - \beta^k_{j+1/2,p})\,\bar{\mathbf{r}}^k_{j+1/2,p}\\ &-\sum_{p=1}^{2}\frac{\Delta t}{\Delta x}\frac{1}{2}\phi\left(\theta^k_{j+1/2,p}\right)\left(\operatorname{sign}(\nu^k_{j,p}) - \nu^k_{j,p}\right)\left(\alpha^k_{j+1/2,p}\lambda^k_{j+1/2,p} - \beta^k_{j+1/2,p}\right)\bar{\mathbf{r}}^k_{j+1/2,p}\\ &+\sum_{p=1}^{2}\frac{\Delta t}{\Delta x}\frac{1}{2}\phi\left(\theta^k_{j-1/2,p}\right)\left(\operatorname{sign}(\nu^k_{j-1,p}) - \nu^k_{j-1,p}\right)\left(\alpha^k_{j-1/2,p}\lambda^k_{j-1/2,p} - \beta^k_{j-1/2,p}\right)\bar{\mathbf{r}}^k_{j-1/2,p}.\end{aligned} \tag{21}$$

Here, $\phi(\theta) = \max(0, \max(\min(2\theta, 1), \min(\theta, 2)))$ is known as the superbee limiter function, and for each cell I_j, we define

$$\theta_{j+1/2,p} = \frac{\alpha_{j,p}\lambda_{j,p} - \beta_{j,p}}{\alpha_{j',p}\lambda_{j',p} - \beta_{j',p}}, \quad j' = j - \operatorname{sign}(\lambda_{j,p}), \quad \nu_{j,p} = \frac{\Delta t}{\Delta x}\lambda_{j,p}.$$

The last two terms in Eq. (21) are the second-order corrections. See Ref. 25 for more details, where the reader can also find the sonic entropy fix that is usually done for Roe-type upwind schemes and that has also been implemented here. In the case where $\lambda_{j-1,p} < 0 < \lambda_{j,p}$, $\lambda_{j-1/2,p}$ in the first term of Eq. (21) is replaced by $\lambda^r_{j-1/2,p} = \lambda_{j,p}\,(\lambda_{j-1/2,p} - \lambda_{j-1,p})/(\lambda_{j,p} - \lambda_{j-1,p})$. Symmetrically, if $\lambda_{j,p} < 0 < \lambda_{j+1,p}$, $\lambda_{j+1/2,p}$ in the second term of Eq. (21), $\lambda_{j+1/2,p}$ is replaced by $\lambda^\ell_{j+1/2,p} = \lambda_{j,p}\,(\lambda_{j+1,p} - \lambda_{j+1/2,p})/(\lambda_{j+1,p} - \lambda_{j,p})$.

2. The adjoint problem

The adjoint problem can be written in quasilinear form as

$$\begin{pmatrix}\lambda\\ \mu\end{pmatrix}_t + \begin{pmatrix}0 & c^2-u^2\\ 1 & 2u\end{pmatrix}\begin{pmatrix}\lambda\\ \mu\end{pmatrix}_x = \begin{pmatrix}-\dfrac{u}{\sigma h}\mathscr{M}^*(\mathscr{M}u - \hat{u}) + \left[-\dfrac{gh}{\sigma}\sigma_x + gB_x + gn^2u\left(\dfrac{2h - \sigma/3}{\sigma h\,R^{1/3}}|u| - \dfrac{2|u|}{R^{4/3}}\right)\right]\mu\\ \dfrac{1}{\sigma h}\mathscr{M}^*(\mathscr{M}u - \hat{u}) + \dfrac{gn^2}{R^{4/3}}2|u|\mu\end{pmatrix}, \tag{22}$$

where $\hat{u}$ is the observed velocity in space and time. We note that λ has units of velocity and μ is non-dimensional. On the contrary, $\mathscr{M}$ is the observation operator defined in Eq. (10), and $\mathscr{M}^*(\mathscr{M}u - \hat{u})$ is given in units of squared velocity.

The final conditions in Eqs. (14) and (15) are given at time $t = T$, and the solution is computed backwards in time from $t = T$ to $t = 0$. In addition, we note that the coefficient matrix

$$A^* = \begin{pmatrix}0 & c^2-u^2\\ 1 & 2u\end{pmatrix}$$

is the transpose of the coefficient matrix in the direct problem. The eigenvalues are the same, and the corresponding eigenvectors are

$$\mathbf{r}_1^* = \begin{pmatrix}-\bar{u} - \bar{c}\\ 1\end{pmatrix} \text{ and } \mathbf{r}_2^* = \begin{pmatrix}-\bar{u} + \bar{c}\\ 1\end{pmatrix}.$$

Analogous to the direct problem, the finite difference of the solution variable $\Delta\mathbf{W}^* = (\Delta\lambda, \Delta\mu)^T$ and the linearized source terms

$$\Delta x\,\mathbf{S}^* = \begin{pmatrix}-\dfrac{\bar{u}\,\Delta x\,M^*(\mathscr{M}u - \hat{u})}{\bar{\sigma}\bar{h}} + \left[-\dfrac{g\bar{h}}{\bar{\sigma}}\Delta\sigma + g\Delta B + gn^2\bar{u}\left(\dfrac{2\bar{h} - \bar{\sigma}/3}{\bar{\sigma}\bar{h}\,\bar{R}^{1/3}}|\bar{u}| - \dfrac{2|\bar{u}|}{\bar{R}^{4/3}}\right)\right]\bar{\mu}\\ \dfrac{1}{\bar{\sigma}\bar{h}}\overline{\mathscr{M}^*(\mathscr{M}u - \hat{u})} + \dfrac{gn^2}{\bar{R}^{4/3}}|2\bar{u}|\bar{\mu}\end{pmatrix}, \tag{23}$$

where

$$\bar{\mu} = \frac{\mu_\ell + \mu_r}{2}, \quad \overline{\mathscr{M}^*(\mathscr{M}u\hat{u})} = \frac{\mathscr{M}^*(\mathscr{M}u_\ell - \hat{u}_\ell) + \mathscr{M}^*(\mathscr{M}u_r - \hat{u}_r)}{2}$$

are decomposed as

$$\Delta\mathbf{W}^* = \alpha_1^*\bar{\mathbf{r}}_1^* + \alpha_2^*\bar{\mathbf{r}}_2^*, \quad \Delta x\hat{\mathbf{S}}^* = \beta_1^*\bar{\mathbf{r}}_2^* + \beta_1^*\bar{\mathbf{r}}_2^*.$$

Here, the coefficients in the decompositions are given by

$$\alpha_1^* = \frac{(-\bar{u}+\bar{c})\Delta\mu - \Delta\lambda}{2\bar{c}}, \quad \beta_1^* = \frac{(-\bar{u}+\bar{c})\bar{S}_2^* - \bar{S}_1^*}{2\bar{c}},$$
$$\alpha_2^* = \frac{(\bar{u}+\bar{c})\Delta\mu + \Delta\lambda}{2\bar{c}}, \quad \beta_2^* = \frac{(\bar{u}+\bar{c})\bar{S}_2^* + \bar{S}_1^*}{2\bar{c}}.$$

The corresponding numerical scheme for the adjoint problem solved backward in time is given by

$$\begin{aligned}
\mathbf{W}_j^{*,k} = \mathbf{W}_j^{*,k+1} &+ \frac{\Delta t}{\Delta x} \sum_{\lambda_{j-1/2,p}^{k+1}>0} (\alpha_{j-1/2,p}^{*,k+1}\lambda_{j-1/2,p}^{k+1} - \beta_{j-1/2,p}^{*,k+1})\,\mathbf{r}_{j-1/2,p}^{*,k+1} \\
&+ \frac{\Delta t}{\Delta x} \sum_{\lambda_{j+1/2,p}^{k+1}<0} (\alpha_{j+1/2,p}^{*,k+1}\lambda_{j+1/2,p}^{k+1} - \beta_{j+1/2,p}^{*,k+1})\,\mathbf{r}_{j+1/2,p}^{*,k+1} \\
&- \sum_{p=1}^{2} \frac{\Delta t}{\Delta x}\frac{1}{2}\phi\left(\theta_{j+1/2,p}^{*,k+1}\right)\left(\mathrm{sign}(\nu_{j,p}^{k+1}) - \nu_{j,p}^{k+1}\right) \\
&\times \left(\alpha_{j+1/2,p}^{*,k+1}\lambda_{j+1/2,p}^{k+1} - \beta_{j+1/2,p}^{+,k+1}\right)\mathbf{r}_{j+1/2,p}^{*,k+1} \\
&+ \sum_{p=1}^{2} \frac{\Delta t}{\Delta x}\frac{1}{2}\phi\left(\theta_{j-1/2,p}^{*,k+1}\right)\left(\mathrm{sign}(\nu_{j-1,p}^{k+1}) - \nu_{j-1,p}^{k+1}\right) \\
&\times \left(\alpha_{j-1/2,p}^{*,k+1}\lambda_{j-1/2,p}^{k+1} - \beta_{j-1/2,p}^{*,k+1}\right)\mathbf{r}_{j-1/2,p}^{*,k+1},
\end{aligned} \tag{24}$$

where

$$\theta_{j+1/2,p}^* = \frac{\alpha_{j,p}^*\lambda_{j,p} - \beta_{j,p}^*}{\alpha_{j',p}^*\lambda_{j',p} - \beta_{j',p}^*}.$$

V. TEST PROBLEMS

The above technique is numerically tested in this section. The direct problem often involves bathymetries consisting of a bump or a channel's throat by which the fluid passes through. Depending on the parameter regime, the flow may accelerate/decelerate and reduce/increase its cross-sectional wet area as it passes through the bump and/or throat. We consider here different situations to show the merits and robustness of the algorithm.

A. Numerical setup and boundary conditions

The inverse problem consists of inferring the bathymetry B and Manning's friction coefficient n from the transient velocity $u(x, t)$. We assume that the velocity is observed at all spatial positions and at all times. That is, the velocity data are assumed to be available at all grid points and at all times. For the direct problem, we initially specify the total height w and the velocity u. Such data are assumed to be known at $t = 0$. At each step, the estimated bathymetry is used to obtain the initial depth $h = w - B$. Regarding the adjoint problem, which is solved backwards in time, here, we impose zero Dirichlet final conditions.

At the left boundary, a discharge Q_{left} and a surface elevation w_{left} are specified at inflow and are extrapolated at outflow for the direct problem. An inflow/outflow at the left boundary occurs when the eigenvalues of the coefficient matrix are positive/negative. At the right boundary, a discharge Q_{right} and a surface elevation w_{right} are specified at inflow and extrapolated at outflow. An inflow/outflow at the right boundary occurs when the eigenvalues of the coefficient matrix are negative/positive. The adjoint problem is used to compute the gradient ∇J. Zero Neumann boundary conditions are implemented for the adjoint variables λ, μ. We assume we know the bathymetry elevation at the boundaries, and we prescribe them to be $B_{\text{in}} = B_{\text{out}} = 0$ at both ends.

We quantify the error and the relative error with the L^∞ norm, and are given by

$$e = \sup_x |B_{\text{approx}}(x) - B_{\text{exact}}|, \text{ and } e_{\text{rel}} = \frac{e}{\sup_x |B_{\text{exact}}(x)|},$$

where B_{approx} and B_{exact} are the approximated and exact bathymetries.

The time window $[0, T]$ where both the direct and the adjoint problems are solved need to be chosen carefully. The end time T needs to be large enough to have the needed information to invert the problem. However, if T is too large, it induces strong interactions with the boundary, where the bathymetry is prescribed. In any case, we have found that the bathymetry estimation is not very sensitive to the end time. We use T as estimated for the linear case in Sec. II B, except for the cases where the Manning's friction coefficient is also estimated.

B. Bathymetry bump

The synthetic data in this first numerical test is obtained with a particular choice of a bathymetry elevation and channel's geometry. The exact bathymetry to be estimated is given by

$$B_{\text{exact}}(x) = \begin{cases} \frac{1}{2}\left(1 - \left(4\left(x - \frac{1}{2}\right)\right)^2\right) + 0.02\sin\left(16\pi\left(x - \frac{1}{4}\right)\right) \\ \quad \text{if } x \in [0.25, 0.75], \\ 0 \\ \quad \text{if } x \in [0,1]\backslash[0.25, 0.75]. \end{cases} \tag{25}$$

The channel's width is given by

$$\sigma(x) = 2\min\left(2.4(x-0.5)^2 + 0.35, 0.5\right). \tag{26}$$

The 3D view of the channel is shown in the left panel of Fig. 2. Following Ref. 14, the Manning's friction coefficient is fixed to $n = 0.009\,\mathrm{s\,m^{-1/3}}$ in this numerical test, and the bathymetry is the only model's parameter to estimate.

We first test the algorithm in a simple setting. In particular, the velocity considered here corresponds to a subcritical smooth steady state (in the absence of friction). Smooth steady states are characterized by two invariants. Namely, the discharge $Q = hu$ and the energy $E = \frac{1}{2}u^2 + g(h + B)$ are both constant throughout the domain when the friction coefficient n vanishes. One could use such invariants to estimate the bathymetry. However, the algorithm presented here is designed for transient flows as well, and the setting in this numerical experiment is meant to test the accuracy in the approximated bathymetry. Given the bathymetry B, a corresponding steady state may be computed by specifying two quantities. Here, we specify the discharge $Q_{\text{in}} = 1$ at inflow at the left boundary and the total height $w_{\text{out}} = B_{\text{out}} + h_{\text{out}} = 1.5$ at

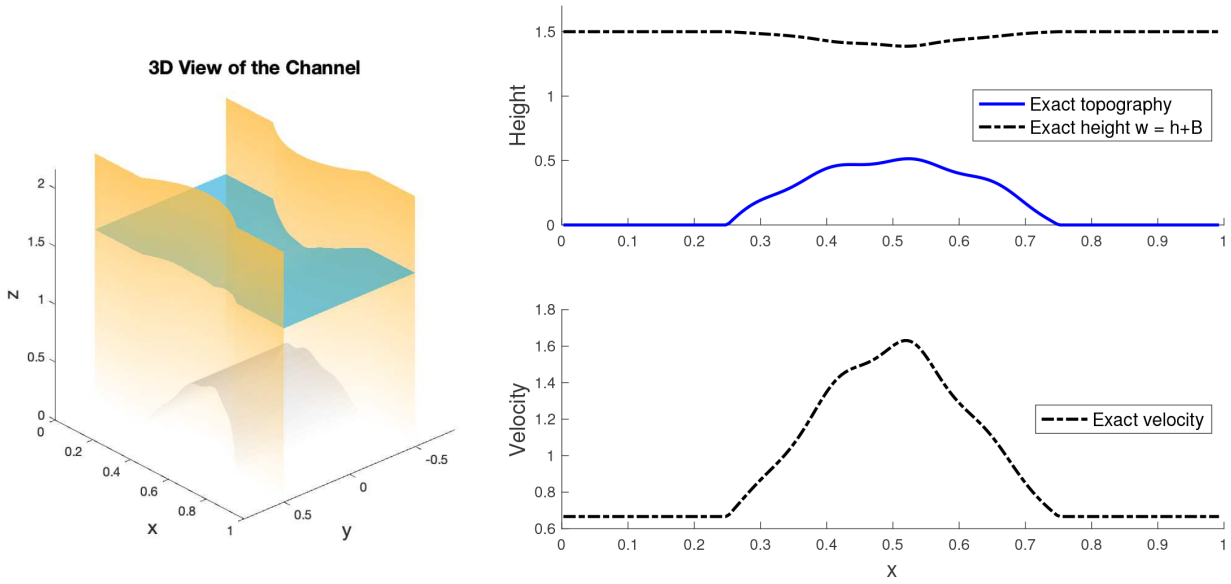

FIG. 2. Left panel: 3D view of the channel. Top right panel: Exact total height $w = h + B$ (black dashed line) and bathymetry (blue solid line) are shown. Bottom right panel: Velocity as a function of x. The solution corresponds to a steady state with discharge $Q_{\text{in}} = 1$ at inflow (left boundary) and total height $w_{\text{out}} = 1.5$ at outflow (right boundary).

outflow at the right boundary. Figure 2 shows the total height $w = h + B$ and exact bathymetry B in the top right panel, while the bottom right panel shows the exact velocity that is observed.

In general, the initial guess needs to be close enough to the target in order to converge to the correct state. However, here, we test the robustness of the algorithm by considering an initial guess $B_o = 0$. The numerical results for the inverse problem are given in Fig. 3. In the left panel, the exact solution is identified with the solid blue line, while the initial guess is denoted by the black dashed line. The final approximation is computed using 80 steps in the algorithm described in Sec. III B and a resolution of 200 grid points.

Taking a characteristic depth $H = 1.5$, domain size $L = 1$, and $g = 9.81$, the time for linear identifiability is $T = L/\sqrt{gH} = 0.26$. The direct and adjoint problems are then solved in the time window $[0, T]$. In the panel, we show the estimation of the bathymetry for the steps 0, 20, 40, 60, and 80. The final step is not easy to distinguish because it is very close to the target. The error is shown in the right panel. The maximum error is $e = 9.1 \times 10^{-3}$, which corresponds to a relative error of $e_{\text{rel}} = 1.77\%$. The maximum error is located near the left boundary. Away from that region, the error is reduced to 2.9×10^{-3}, which corresponds to a relative error of 0.57%.

C. A transient flow with friction

The ultimate goal in this work is to estimate the bathymetry in transient flows. For that end, the observed velocity in these numerical tests is time dependent, and the synthetic data are constructed as follows. Given the bathymetry in Eq. (25), the initial condition in the direct problem is the smooth supercritical steady state associated with the discharge $Q_{\text{steady}} = 8$ and the total height $w_{\text{out}} = B_{\text{out}} + h_{\text{out}} = 1$. However, the discharge imposed at the left boundary is $Q_{\text{in}} = 9.6$, which is 20% higher compared to that corresponding to the steady state. The resulting transient flow consists of a perturbation to a steady state. The right-going shockwave propagates and passes through the bump in the bathymetry. This generates a time-dependent velocity, which is used as the synthetic data in the adjoint problem.

Taking a characteristic depth $H = 2$, domain size $L = 1$, and $g = 9.81$, the time for linear identifiability is $T = L/\sqrt{gH} = 0.23$. This is our end time for this numerical test. The Manning's friction coefficient here is fixed to $n = 0.009\,\text{s}\,\text{m}^{-1/3}$. Figure 4 shows the approximated bathymetry in steps 1–3 and 45 in the left panel. For completeness, the error is exhibited in the right panel. The maximum error in the last step (away from the left boundary) is $e = 7.2 \times 10^{-3}$,

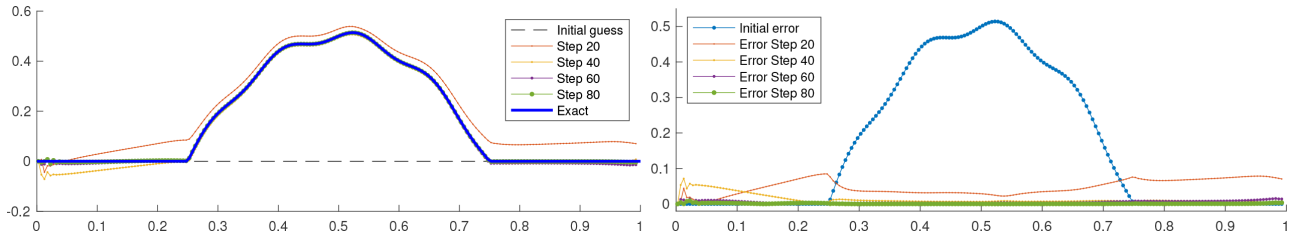

FIG. 3. Left panel shows the exact bathymetry (solid blue line) given by Eq. (25), the initial guess $B_o = 0$ (black dashed line) and the intermediate steps (dotted lines in different colors and mark sizes). The right panel shows the error $|B_n - B_{\text{exact}}|$ at steps 20, 40, 60, and 80.

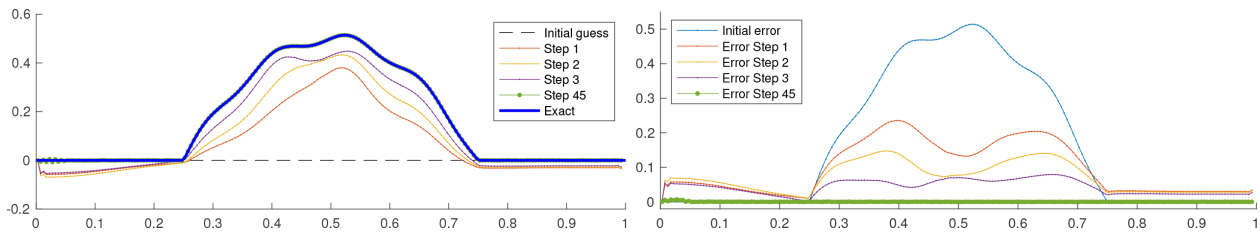

FIG. 4. Left panel: Exact bathymetry (blue solid line), the initial guess (black dashed line), and the intermediate steps in the algorithm (dotted lines). Right panel: Error in steps 1–3 and 45.

which corresponds to a relative error of $e_{\text{rel}} = 1.39\%$. Away from that region, the error is reduced to 1.1×10^{-3}, which corresponds to a relative error of 0.21%. Flows in realistic applications may not be in steady-state equilibrium. Estimating the bathymetry from transient velocity measurements is a lot more challenging compared to a situation where the flow corresponds to a steady state. The present algorithm has shown to be efficient in those circumstances.

Figure 5 shows the time evolution of the total height (left column) and velocity (right column) at times $t = 0.003\,6, 0.035\,55$, and 0.08. The total height is computed both using the exact and the approximated bathymetries. The exact total height is denoted by the dashed blue line, while the approximated solution is identified with the dashed red line. The steady-state total height is also shown for reference (black dotted line). The exact and approximated topographies are denoted by the solid blue and dotted red lines, respectively. The approximated solution is very accurate even in this time-dependent problem, and the differences are hard to be distinguished.

D. Bump in a channel with varying width, friction, and discontinuous top surface

Discontinuous weak solutions of hyperbolic systems like the shallow water equations may appear in finite time. The robustness of the algorithm is tested here by estimating the bathymetry from velocity data with discontinuities. The exact bathymetry is given by

$$B(x) = \begin{cases} \frac{1}{4}\left[\cos\left(10\pi\left(x - \frac{1}{2}\right)\right) + 1\right] & \text{if} \quad 0.4 < x \le 0.6, \\ 0, & \text{otherwise}, \end{cases}$$

and the width σ is given by Eq. (26).

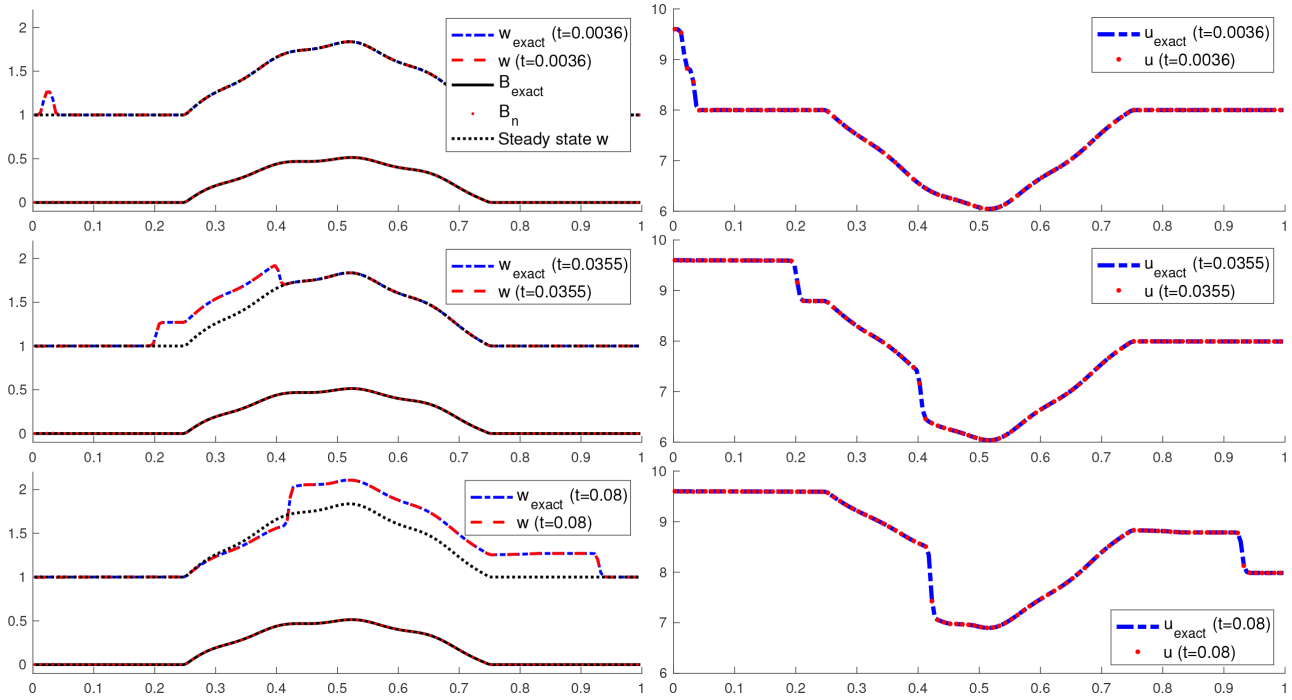

FIG. 5. Left column: Approximated (blue dashed line) and exact (red dashed line) total heights at times $t = 0.0036, 0.0355$, and 0.08 in descending order for the transient flow of Sec. V C. The exact (solid black line) and approximated (dotted red line) bathymetries are also shown. The steady-state height is included to highlight the difference compared to the transient flow (dotted black line). Right column: approximated (dotted red line) and exact (dashed blue line) velocities.

The computed state in this numerical test is a steady state with shockwave in the absence of friction. However, here the Manning's friction coefficient is set to $n = 0.009\,\mathrm{s\,m^{-1/3}}$, following Ref. 14. The initial height at the left and right boundaries are $w_{\text{in}} = 1.1$ and $w_{\text{out}} = 0.75$, respectively. An initial shock is placed at $x_{\text{shock}} = 0.65$ with left and right states given by $w_{\text{left}} = 1.417$, $u_{\text{left}} = 8.085$, and $w_{\text{right}} = 0.931$, $u_{\text{right}} = 12.198$, respectively. The energy is initially piecewise constant, satisfying $E_{\text{in}} = 46.59$ for $x \le x_{\text{shock}}$, and $E_{\text{out}} = 83.52$ for $x > x_{\text{shock}}$. This shockwave is stationary in the absence of friction. The right panel of Fig. 6 shows the 3D view of the channel (yellow surface), the bathymetry B (black surface), and the initial height's elevation w (blue surface).

Taking a characteristic depth $H = 2.5$, domain size $L = 1$, and $g = 9.81$, the time for linear identifiability is $T = L/\sqrt{gH} \approx 0.21$. This is our end time for this numerical test. The top left panel of Fig. 6 shows the estimated bathymetry given by the algorithm in Sec. III B at steps 1–5 and 12. The initial state is $B_o = 0$. This is significantly far from the target, which consists of a bump at the center of the domain. The first step already has a bump-like structure, with a small jump near the shockwave. At step 5, the bathymetry is close to the target, and at the final step 12, the approximation is virtually on top of the exact bathymetry. The error as a function of x is shown in the bottom left panel for different steps, where the convergence to the exact solution is evident. At step 12, the error is below $e = 4.4 \times 10^{-3}$, which corresponds to a relative error of $e_{\text{rel}} = 0.87\%$ of the maximum bathymetry's elevation. We note that the algorithm works well even in the presence of shockwaves and friction.

E. Bathymetry and Manning's friction coefficient inversion

In this test, we invert both the bathymetry and the Manning's friction coefficient simultaneously. Although the value of n in Sec. V D is realistic, it may not have a strong effect in the flow in the time window considered here. As a sensitivity test, we have increased the target value of the exact Manning's friction coefficient to $n_{\text{exact}} = 0.027\,\mathrm{s\,m^{-1/3}}$, which is three times larger compared to the previous one. We chose a smaller time window with $T = 0.02$. However, in this case, it took 2000 iteration steps to converge to the exact solution with an error of $e = 3.9 \times 10^{-3}$, which corresponds to a relative error of $e_{\text{rel}} = 0.77\%$ of the maximum bathymetry's elevation.

Using the same symbols as in Fig. 6, the top left panel of Fig. 7 shows the exact bathymetry, and the approximated bathymetry at the initial and intermediate steps 101, 201, 301, 401, and 2000. The error is shown in the bottom left panel. Although it took many more steps, the error at the final step is very small.

We can simultaneously estimate both the bathymetry's elevation and the Manning's friction coefficient in the algorithm in Sec. III B. The second component of the gradient ∇J has the approximated friction coefficient n as a factor itself. As a result, the initial value cannot be zero because it represents an equilibrium value in the algorithm. We set the initial value of the Manning's friction coefficient as $n_o = 0.0027 = \frac{1}{10} n_{\text{exact}}$. The bottom right panel of Fig. 7 shows the estimated Manning's friction coefficient as a function of step number. The estimated value is already close to the exact value after about 20 steps. We only show 200 steps to see the variations in the early steps. However, the plot for 2000 steps (not shown) shows a convergence to the exact value.

The top right panel of Fig. 7 shows the bathymetry B and the initial surface elevation with a shockwave used in the present numerical test and the previous Sec. V D. The algorithm provides very accurate results in flows with or without friction, steady or transient states, with initial guesses that are significantly far from the exact solutions.

F. Manning's coefficient inversion in the presence of wet-dry states

The numerical test in this last section is motivated by laboratory experiments of dam breaks conducted in converging/diverging channels. See, for instance, Chap. 5 of the book[14] for a list of experiments

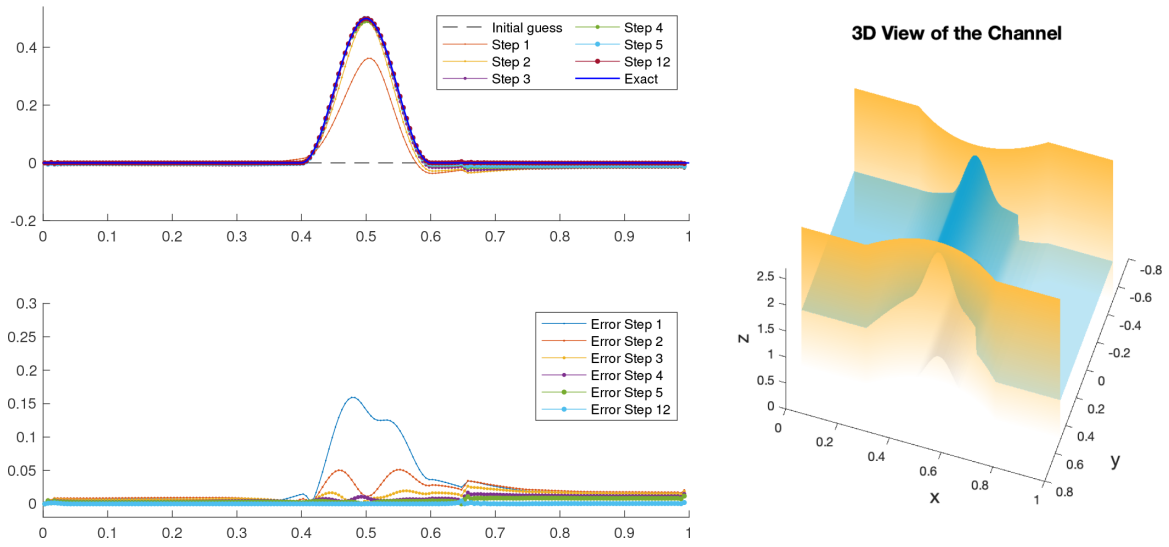

FIG. 6. Top left panel: Exact bathymetry (blue solid line), the initial guess (black dashed line), and the intermediate steps in the algorithm (dotted lines). Bottom left panel: Error in steps 1–5 and 12. Right panel: 3D view of the channel (yellow surface), the exact bathymetry (black surface), and the initial surface elevation $w = B + h$ (blue surface).

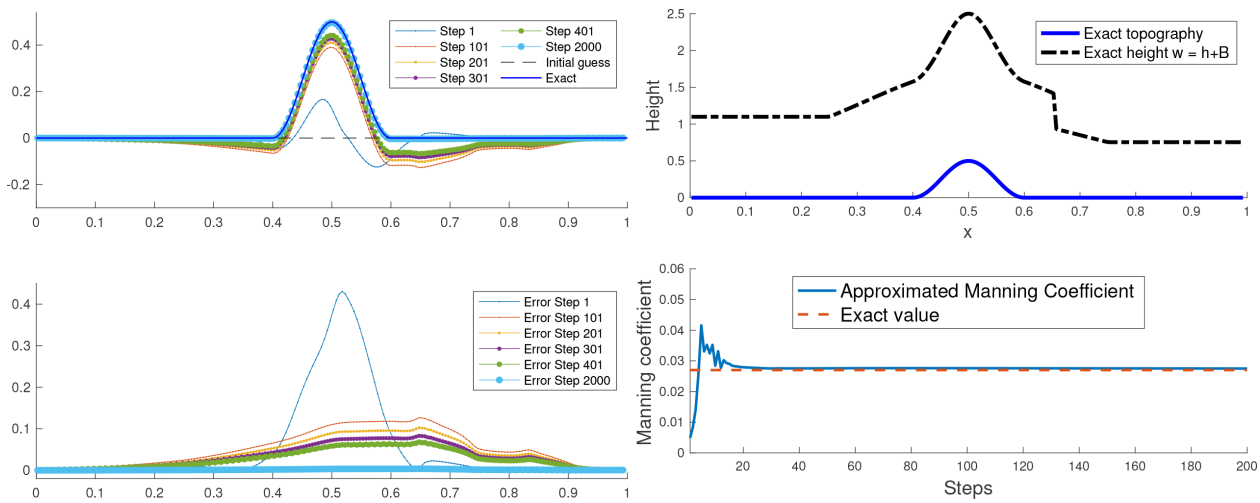

FIG. 7. Top left panel: Exact bathymetry (blue solid line), the initial guess (black dashed line), and the intermediate steps in the algorithm (dotted lines). Bottom left panel: Error in steps 1, 101, 201, 301, 401, and 2000. Top right panel: The exact topography (solid blue line) and the exact total height (black dashed line) are displayed. Bottom right panel: The approximated Manning's friction coefficient is shown as a function of iteration step (solid blue line), and the exact coefficient is included for reference in the dashed red line.

in channels with different bed slopes and different wet and dry conditions. The experiments in Ref. 14 Sec. 5.3.4 were taken from Ref. 26. The channel has vertical walls and width variations along the x-axis, approximately given by the graph in the left panel of Fig. 8. The channel's length is 21.2 m, and its width is 1.4 m from 0 to 5 m, and from 16.8 to 21.2 m. The minimum width is 0.6 m at $x_m = 8.5$ m.

In the experiment, the flow is initially given by

$$u(x, t=0) = 0, w(x, t=0) = \begin{cases} 0.3\,\text{m} & \text{if} \quad x < x_m = 8.5\,\text{m}, \\ H_{\text{out}} = 10^{-5}\,\text{m}, & \text{otherwise}, \end{cases} \tag{27}$$

which corresponds to a flow initially at rest, where the downstream part of the channel is dry (a threshold value of $H_{\text{out}} = 10^{-5}$ has been used). The gate is assumed to be instantaneously removed. The left boundary is a solid wall. We have used zero Dirichlet left boundary conditions in the velocity and Neumann left boundary conditions for the height. The right boundary extrapolates the data at outflow and imposes H_{out} at inflow. Once the dam breaks, the flow evolves as illustrated in the left panel of Fig. 9 at $t = 4$ s. The resolution here is $\Delta x = 21.2\,\text{m}/200$.

The bathymetry is flat $B = 0$. So, we are interested in estimating the Manning's friction coefficient, which is unknown. Unfortunately, the depth at two locations (P_1 and P_2 in Fig. 9) are the only quantities reported in this experiment. In Ref. 27, it was found that one good approximation for the Manning's friction coefficient is $n = 0.0084\,\text{s}\,\text{m}^{-1/3}$. Here, we create synthetic velocity data based on this value to approximate the friction coefficient based on those velocity measurements. The purpose of this numerical test is to show that the algorithm works well even in the presence of wet–dry states, in connection with the above experiment.

The approximated Manning's coefficient is shown for different steps in the left panel of Fig. 9. One can observe that the Manning's coefficient is very close to the exact value after 20 steps in the algorithm. The approximated values were obtained using a time window $[0, T]$ with $T = 4$ s before the flow reaches the boundaries. We note that the amplitude in Eq. (17) is chosen much smaller here ($\alpha = 5 \times 10^{-4}$) in this case, where both bathymetry and friction are estimated simultaneously in the presence of wet and dry states.

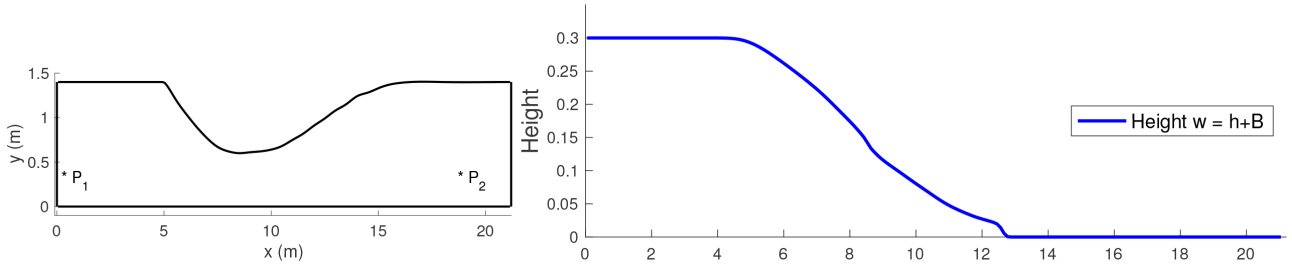

FIG. 8. Left panel: Approximated channel's width as a function of x (top view of the channel). The points P_1 and P_2 indicate the locations where the depth was measured in the corresponding experiment in Ref. 14. Right panel: Total height $w = h + B$ at time $t = 4$ s with initial conditions (27) and the boundary conditions below.

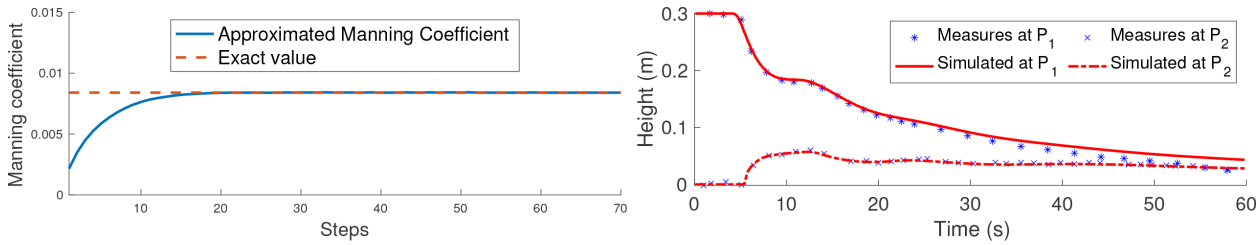

FIG. 9. Left panel: Convergence of the Manning's friction coefficient to the correct value. The approximations are plotted for different steps. Right panel: Comparison between experimental data and the numerical approximation obtained by the present schemes of the water's height at two particular locations in x, vs time. The left point is located at the left boundary $P_1 = 0$, and the right point is located at $P_2 = 18.5$ m.

In the experimental data in Refs. 14 and 26, the height was measured in time at two particular locations. One at the left boundary $P_1 = 0$, and the other one near the right boundary $P_2 = 18.5$ m. The right panel in Fig. 9 compares the real and numerical values. We observe a good agreement, especially at the location P_2 near the right boundary, for the entire simulation. The numerical approximation at P_1 is accurate for the first part of the simulation, and overestimates it for the second half. Boundary conditions and the adjustment of the Manning coefficient might affect the predictions.

VI. CONCLUSIONS

In this work, we formulated a constrained optimization problem to estimate the bed channel bathymetry and Manning's friction coefficient from available data of the fluid's velocity. The continuous problem is first presented and analyzed. A quadratic functional, which by means of Lagrange multipliers incorporates the shallow water equations, is minimized using the Fréchet derivative. We proved that the velocity data determine uniquely the derivative of the bathymetry in a linearized shallow water system. That is, we proved that the inverse problem is identifiable in the linearized system, which helped us estimate the time window that is needed for the inverse problem in the nonlinear case, except for the cases where both the bathymetry and the Manning's friction coefficients are estimated simultaneously. A continuous descent method is formulated to obtain the minimal solution. Both direct and adjoint systems are proposed to be solved by a second-order Roe-type upwind numerical scheme. However, the algorithm works for any other efficient and robust numerical scheme. We estimate the bathymetry of transient flows as well as the Manning's friction coefficient. Several benchmark problems are presented in order to verify the numerical performance of the proposed method. A simple steady-state case is first formulated to verify the reliability of the algorithm before transient flows can be treated. In this first case, we considered a steady-state velocity and a bathymetry bump with a sinusoidal perturbation. In a second test, we considered a transient flow consisting of a right-going perturbation to a steady state. Finally, we simultaneously estimated both the bathymetry and the Manning's friction coefficient in a channel with varying width and discontinuous top surface, and a numerical test was presented to estimate the Manning's coefficient in the presence of wet–dry states, motivated by experimental data. We obtained very accurate approximations of the bathymetry in all cases.

We have provided an algorithm that works very well even in transient flows in channels with vertical walls of varying width, discontinuous top surfaces, and even wet–dry states. The need for a good initial guess and the empirical initial coefficient (α_k) in the search direction are often limitations for approaches like the one presented here. However, we have shown that our algorithm is not very sensitive to those parameters, and we provided criteria to choose the best coefficient α_k together with conditions to stop our algorithm. Furthermore, our setting is flexible and may be adapted to estimate other parameters or systems.

From a theoretical perspective, the continuous descent method in Sec. III can be extended to higher dimensions on irregular domains. However, the computational complexity is much greater. We aim to report on these in future works.

The identifiability result in Sec. II for the linear shallow water equation is local. That is, for identifying bathymetry in an interval of length L, we need data only in that interval with a final time greater than $T = L/\sqrt{gH}$. We use the same time and data for the nonlinear case based on Theorems 1 and 2. We conjecture that the local identification is valid for smooth flows before shocks are formed. We clarify that in this work we assume that the velocity observations are available at all grid points for simplicity in the computation of the source term in the adjoint equations. It is open to determine the minimal data required for identification. These are challenging research problems to be addressed in future works.

ACKNOWLEDGMENTS

This research was supported, in part, by grants UNAM-DGAPA-PAPIIT IN112222 and Conacyt A1-S-17634. This research was supported, in part, by grants UNAM-DGAPA-PAPIIT IN112222 and Conacyt A1-S-17634. The co-author G. H-D would like to thank the hospitality of NorthWest Research Associates and the support of UNAM-PASPA-DGAPA during his sabbatical visit.

The authors acknowledge the anonymous reviewers for their constructive comments which helped us to improve the manuscript.

AUTHOR DECLARATIONS

Conflict of Interest

The authors have no conflicts to disclose.

Author Contributions

Gerardo Hernández-Dueñas: Conceptualization (equal); Formal analysis (equal); Investigation (equal); Methodology (equal); Software (lead); Visualization (lead); Writing – original draft (equal); Writing – review & editing (lead). **Miguel Angel Moreles:** Conceptualization (equal);

Formal analysis (equal); Investigation (equal); Methodology (equal); Project administration (lead); Software (supporting); Visualization (supporting); Writing – original draft (equal); Writing – review & editing (equal). **Pedro Gonzalez Casanova:** Conceptualization (equal); Formal analysis (equal); Investigation (equal); Methodology (equal); Software (supporting); Visualization (supporting); Writing – original draft (equal); Writing – review & editing (equal).

DATA AVAILABILITY

Data sharing is not applicable to this article as no new data were created or analyzed in this study.

REFERENCES

[1]G. K. Vallis, *Atmospheric and Oceanic Fluid Dynamics* (Cambridge University Press, 2017).
[2]M. Sellier, "Inverse problems in free surface flows: A review," Acta Mech. **227**, 913–935 (2016).
[3]R. J. LeVeque, D. L. George, and M. J. Berger, "Tsunami modelling with adaptively refined finite volume methods," Acta Numer. **20**, 211–289 (2011).
[4]M. E. Vázquez-Cendón, "Improved treatment of source terms in upwind schemes for the shallow water equations in channels with irregular geometry," J. Comput. Phys. **148**, 497–526 (1999).
[5]K. Marks and P. Bates, "Integration of high-resolution topographic data with floodplain flow models," Hydrol. Processes **14**, 2109–2122 (2000).
[6]R. M. Westaway, S. N. Lane, and D. M. Hicks, "Remote sensing of clear-water, shallow, gravel-bed rivers using digital photogrammetry," Photogramm. Eng. Remote Sens. **67**, 1271–1281 (2001).
[7]N.-R. Kevlahan, R. Khan, and B. Protas, "On the convergence of data assimilation for the one-dimensional shallow water equations with sparse observations," Adv. Comput. Math. **45**, 3195–3216 (2019).
[8]Y. Ding, Y. Jia, and S. S. Wang, "Identification of Manning's roughness coefficients in shallow water flows," J. Hydraul. Eng. **130**, 501–510 (2004).
[9]Y. Ding and S. S. Wang, "Identification of Manning's roughness coefficients in channel network using adjoint analysis," Int. J. Comput. Fluid Dyn. **19**, 3–13 (2005).
[10]Y. Ding and S. S. Wang, "Optimal control of flood diversion in watershed using nonlinear optimization," Adv. Water Resour. **44**, 30–48 (2012).
[11]S. Kar and A. Guha, "Letter: Ocean bathymetry reconstruction from surface data using hydraulics theory," Phys. Fluids **30**, 121701 (2018).
[12]P. Garcia-Navarro and M. E. Vazquez-Cendon, "On numerical treatment of the source terms in the shallow water equations," Comput. Fluids **29**, 951–979 (2000).
[13]M. J. Castro, J. A. García-Rodríguez, J. M. González-Vida, J. Macías, C. Parés, and M. E. Vázquez-Cendón, "Numerical simulation of two-layer shallow water flows through channels with irregular geometry," J. Comput. Phys. **195**, 202–235 (2004).
[14]A. A. Khan and W. Lai, *Modeling Shallow Water Flows Using the Discontinuous Galerkin Method* (CRC Press, 2014).
[15]M. Bolognesi, G. Farina, S. Alvisi, M. Franchini, A. Pellegrinelli, and P. Russo, "Measurement of surface velocity in open channels using a lightweight remotely piloted aircraft system," Geomatics, Natural Hazards Risk **8**, 73–86 (2017).
[16]L. Hörmander, *Lectures on Nonlinear Hyperbolic Differential Equations* (Springer Science & Business Media, 1997), Vol. 26.
[17]T.-P. Liu and T. Yang, "Weak solutions of general systems of hyperbolic conservation laws," Commun. Math. Phys. **230**, 289–327 (2002).
[18]E. W. Cheney, E. Cheney, and W. Cheney, *Analysis for Applied Mathematics* (Springer, 2001), Vol. 1.
[19]G. Hernández-Dueñas and S. Karni, "Shallow water flows in channels," J. Sci. Comput. **48**, 190–208 (2011).
[20]A. Kurganov and G. Petrova *et al.*, "A second-order well-balanced positivity preserving central-upwind scheme for the Saint-Venant system," Commun. Math. Sci. **5**, 133–160 (2007).
[21]J. Balbás and S. Karni, "A central scheme for shallow water flows along channels with irregular geometry," ESAIM: Math. Modell. Numer. Anal. **43**, 333–351 (2009).
[22]P. L. Roe, "Approximate Riemann solvers, parameter vectors, and difference schemes," J. Comput. Phys. **43**, 357–372 (1981).
[23]M. E. Hubbard and P. Garcia-Navarro, "Flux difference splitting and the balancing of source terms and flux gradients," J. Comput. Phys. **165**, 89–125 (2000).
[24]P. Roe, "Upwind differencing schemes for hyperbolic conservation laws with source terms," in *Nonlinear Hyperbolic Problems* (Springer, 1987), pp. 41–51.
[25]R. J. Leveque, *Numerical Methods for Conservation Laws* (Springer, 1992), Vol. 3.
[26]C. Bellos, V. Soulis, and J. Sakkas, "Experimental investigation of two-dimensional dam-break induced flows," J. Hydraul. Res. **30**, 47–63 (1992).
[27]G. Hernandez-Duenas and A. Beljadid, "A central-upwind scheme with artificial viscosity for shallow-water flows in channels," Adv. Water Resour. **96**, 323–338 (2016).